ACS APPLIED MATERIALS & INTERFACES

Research Article

Cite This: ACS Appl. Mater. Interfaces 2019, 11, 4219−4225

www.acsami.org

Highly Efficient Transparent Nanophosphor Films for Tunable White-Light-Emitting Layered Coatings

Dongling Geng, Gabriel Lozano,* and Hernán Míguez*

Instituto de Ciencia de Materiales de Sevilla, Consejo Superior de Investigaciones Científicas-Universidad de Sevilla (CSIC-US), C/Américo Vespucio 49, 41092 Sevilla, Spain

ABSTRACT: Bright luminescence in rare-earth (RE) nanocrystals, the so-called nanophosphors, is generally achieved by choosing a host that enables an effective excitation of the RE activator through charge or energy transfer. Although tungstate, molybdate, or vanadate compounds provide the aforementioned transfer, a comparative analysis of the efficiency of such emitters remains elusive. Herein, we perform a combined structural and optical analysis, which reveals that the tetragonal $GdVO_4$ matrix gives rise to the highest efficiency among the different transparent nanophosphor films compared. Then, we demonstrate that by a sequential stacking of optical quality layers made of Eu^{3+}- and Dy^{3+}-doped nanocrystals, it is possible to attain highly transparent white-light-emitting coatings of tunable shade with photoluminescence quantum yields above 35%. Layering provides a precise dynamic tuning of the chromaticity based on the photoexcitation wavelength dependence of the emission of the nanophosphor ensemble without altering the chemical composition of the emitters or degrading their efficiency. The total extinction of the incoming radiation along with the high quantum yields achieved makes these thin-layered phosphors one of the most efficient transparent white converter coatings ever developed.

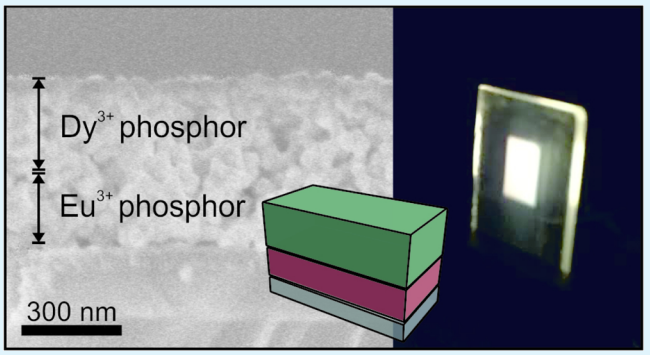

KEYWORDS: *transparent coatings, phosphor materials, rare-earth nanocrystals, nanophosphors, white-light emission*

1. INTRODUCTION

Light-emitting coatings based on rare-earth (RE)-doped phosphors are the key ingredients in recent light-emitting devices.[1] Their robustness lies in the high chemical and thermal stability of their optical performance, which makes them almost insensitive to temperature or environmental changes. The canonical configuration found in most luminaries of this kind consists of an electroluminescent blue-light-emitting diode (LED) used to photoexcite a thick coating of cerium-doped yttrium aluminum garnet (Ce-YAG) crystals, which emits a broad band in the green-to-red region of the visible spectrum.[2] The combination of such photoluminescence (PL) with a part of the incoming blue light that passes through the color converter without being absorbed results in the white light we are accustomed to.

This highly successful approach has, however, certain drawbacks. One of them is that it yields a cool shade of white light, and it is hard to tune the chromaticity of the emission; the other is that it cannot be employed to obtain transparent photoluminescent displays. The reason is the strong diffuse scattering that occurs inside the color-converting layer, which is a disordered packing of large irregular phosphor crystals (several micrometers of average size). The limitations imposed by this lack of transparency have motivated the search for ways to obtain optical-quality Ce-YAG.[3,4] Murai et al. have actually shown that it is possible to synthesize this material in the form of thin films with optical quality. However, the low extinction coefficient at short visible wavelengths hinders the consecution of a balanced white with thin films. Also, a wide variety of matrices have been doped with one or several kinds of RE cations, including glass ceramics, metal organic frameworks, layered hydroxides, and so forth, with the aim of achieving transparency and white emission simultaneously, but low efficiency is achieved in most cases.[5−12] Another approach to prepare transparent phosphor layers is based on the use of RE nanocrystals or nanophosphors. Although transparent, nanophosphor films generally feature low brightness and low quantum yield (QY) because of the small absorption cross section of RE cations and the large surface-to-volume ratio of as-synthesized nanocrystals, which represent the main barriers for practical applications. To improve the emission of these materials, a judicious choice of the inorganic host material along with its crystal structure is central. Indeed, tungstate, molybdate, and vanadate compounds are of special interest in this regard as they enable the excitation of RE cations through energy transfer from the host that is more efficient than the direct excitation, which results in a higher

Received: October 5, 2018
Accepted: December 21, 2018
Published: December 21, 2018

DOI: 10.1021/acsami.8b17368
ACS Appl. Mater. Interfaces 2019, 11, 4219−4225

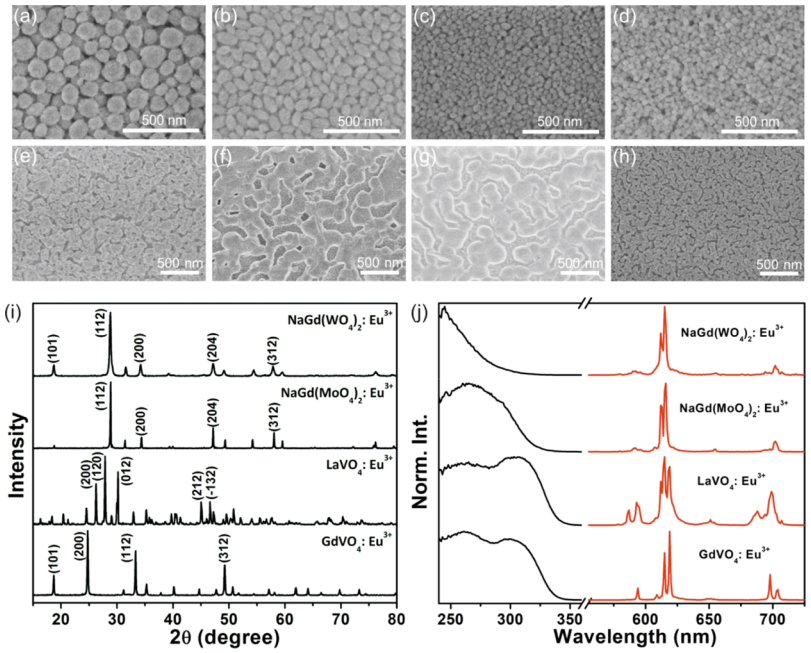

Figure 1. (a–h) SEM images of the top surface of $NaGd(WO_4)_2$:Eu^{3+} (a,e), $NaGd(MoO_4)_2$:Eu^{3+} (b,f), $LaVO_4$:Eu^{3+} (c,g), and $GdVO_4$:Eu^{3+} (d,h) nanophosphor films prepared at room temperature (a–d) and annealed at 800 °C (e–h). (i) XRD patterns and (j) normalized photoexcitation (black line) and emission (red line) spectra for the nanophosphor films annealed at 800 °C.

brightness.[13−16] However, a comparative study of the QY of such compounds is still missing.

In this paper, we describe a synthetic route to attain scattering-free films made of RE-activated $NaGd(WO_4)_2$, $NaGd(MoO_4)_2$, $LaVO_4$, and $GdVO_4$ nanophosphors and perform a systematic evaluation of their performance on the basis of their QY. Then, we use the most efficient host to prepare red- and green-emitting phosphor layers based on Eu^{3+} and Dy^{3+} activators, which, combined in a bilayer structure, yield transparent and efficient phosphor coatings that emit white light. We optimize the thickness of the constituent layers to achieve a total extinction of the incoming photoexcitation as well as a bright white-light emission of tunable shade. The absence of light scattering in the stack provides both transparency and efficient photoexcitation of the inner layers. The shade of the emitted light from a given coating can be continuously tuned without altering the chemical composition of the emitters by means of the gradual shift of the photoexcitation wavelength, a consequence of the spectral dependence of the light penetration depth. The total extinction of the incoming radiation along with QYs above 35% make these layered phosphors one of the most efficient transparent white converter coatings ever developed. Central to this achievement is the formation of a thin (hundreds of nanometers) plane parallel packing of RE nanophosphors by wet deposition methods that was later sintered at a high temperature in a controlled way; hence, transparency was preserved all through the process. As a result, phosphor films displaying simultaneously high QY, bright-colored emission, and transparency are achieved.

2. RESULTS AND DISCUSSION

To prepare thin phosphor films with high optical quality, nanophosphors must feature a small nanoparticle size to avoid light scattering and high colloidal stability in polar solvents to prepare colloidal suspensions that are stable. In particular, nanophosphors employed in our investigation are synthesized following a solvothermal route and polyacrylic acid (PAA) as the functionalization agent, which not only has an important effect on the size and shape of the final nanocrystals but also increases the surface charge value that results in the stability of the suspension. The luminescent properties of nanophosphors arise from the interplay among a variety of factors ranging from composition to crystallinity or surface properties, and it is hard to foresee their efficiency prior to fabrication. We investigate nanophosphors based on $NaGd(WO_4)_2$, $NaGd(MoO_4)_2$, $LaVO_4$, and $GdVO_4$ as inorganic hosts, as these matrices enable the excitation of the activator through an efficient energy transfer from the host to Eu^{3+}, which results in brighter materials. In fact, the absorption bands of RE activators are generally associated to f–f transitions, being spectrally narrow and featuring low absorption cross sections. For this reason, aiming to improve the brightness of these materials, a wise choice of the inorganic host material enables the excitation of the activator through energy transfer from the host. However, such transfer bands lie in the ultraviolet B or ultraviolet C region of the spectrum, where commercial diodes are rather inefficient nowadays, despite the swift increase in the demand for efficient UV light sources for applications that go beyond lighting, such as printing, curing, or disinfection.[17] Figure 1a–d shows a scanning electron micrograph of a top view of such films with controllable thickness and high optical quality.[18,19] Indeed, nanophosphor films are prepared by spin coating using alcoholic dispersions. Our method allows the fabrication of bright, transparent, and efficient thin films using a facile wet deposition route. Notice that compared with other coating techniques such as spray coating, sputtering, or screen printing, spin coating represents a simple and inexpensive alternative to prepare uniform layers of high optical quality with a film thickness that can be accurately controlled. Then, films are annealed at 800 °C—see Figure 1e–h—to improve their emission properties, as both crystallinity and the crystallite size

DOI: 10.1021/acsami.8b17368
ACS Appl. Mater. Interfaces 2019, 11, 4219−4225

enlarge with temperature, yielding higher QY values.[17] In general, the bond length and optical electronegativity of the ligand affect the crystal field strength significantly,[20,21] whereas the varying O−Gd−O or O−La−O bond angle alters the distortions of the GdO_8 or LaO_8 dodecahedron in the structure. Therefore, the choice of the host materials determines the crystal field strength and the lanthanide site, which have a great influence on the PL properties of Eu^{3+}. Figure 1i shows the X-ray diffraction (XRD) patterns recorded for the nanophosphors after sintering at 800 °C. Doped $NaGd(WO_4)_2$, $NaGd(MoO_4)_2$, $LaVO_4$, and $GdVO_4$ particles feature a crystallite size of ∼49, ∼93, ∼81, and ∼73 nm, and grow into tetragonal, tetragonal, monoclinic, and tetragonal structures, respectively, which can be verified by the ICDD files numbered 00-25-0829, 00-25-0828, 01-070-2392, and 01-086-0996. We have included the (*hkl*) index of the different peaks observed in the diffraction patterns, which demonstrates the formation of single host phases. Figure 1j gives the excitation and emission spectra of the nanophosphor films annealed at 800 °C for 4 h. The photoexcitation spectra monitored at the emission peak of Eu^{3+} are composed of a broad and intense band because of the charge transfer within the anions (WO_4^{2-}, MoO_4^{2-}, and VO_4^{3-}) of the matrices and from Eu^{3+} to O^{2-}, which indicates the existence of energy transfer from the hosts to Eu^{3+}. The typical emission profile of Eu^{3+} ions is observed when exciting at 300 nm. We can assign the different bands observed at ∼580, ∼615, ∼650, and ∼700 nm in the PL spectrum of the different nanophosphor films to the characteristic transition lines from the excited $^5D_0$ level to $^7F_1$, $^7F_2$, $^7F_3$, and $^7F_4$ levels of Eu^{3+}, respectively. As these transitions are associated to the activator, all fabricated Eu^{3+} nanophosphor films display similar emission bands in the PL spectra. However, the differences in the symmetry of the lattice site occupied by the activator or the local crystal environment provided by the host give rise to the variations observed in the fine features of the emission spectrum.[22] To evaluate the performance of the different films fabricated, we measure the QY of $NaGd(WO_4)_2$:Eu^{3+}, $NaGd(MoO_4)_2$:Eu^{3+}, $LaVO_4$:Eu^{3+}, and $GdVO_4$:Eu^{3+} nanophosphor films, obtaining 10, 15, 25, and 75%, respectively. This group of nanophosphors allows the comparison of materials with the same crystalline structure but different composition, that is, $NaGd(WO_4)_2$:Eu^{3+}, $NaGd(MoO_4)_2$:Eu^{3+}, and $GdVO_4$:Eu^{3+}, and similar chemical composition but different crystalline structure, that is, $LaVO_4$:Eu^{3+} and $GdVO_4$:Eu^{3+}. Although disparities in the QY values experimentally observed may originate from the different transfer efficiencies between the host and the activator or from the variations in the crystal structure, which affect the radiative rate of the activator, only rigorous calculations of the electronic structure of these materials could provide an ultimate answer for the physical origin of the differences found between the experimental efficiency values.

To attain efficient and tunable white-light-emitting phosphor coatings, the most efficient $GdVO_4$:Eu^{3+} nanophosphor film was employed as the red-emitting sublayer and the Dy^{3+}-doped $GdVO_4$ as the green sublayer. As depicted by the black solid line in Figure 2a, $GdVO_4$:Dy^{3+} nanophosphor features narrow emission lines in the blue (483 nm) and yellow (572 nm) regions of the visible spectrum. By comparing the excitation spectra of $GdVO_4$:Dy^{3+} and $GdVO_4$:Eu^{3+} shown by the dashed lines in Figure 2a, one can notice that they are almost identical, which demonstrates the occurrence of energy transfer from the host to Dy^{3+} ions. Layered phosphor coatings were fabricated

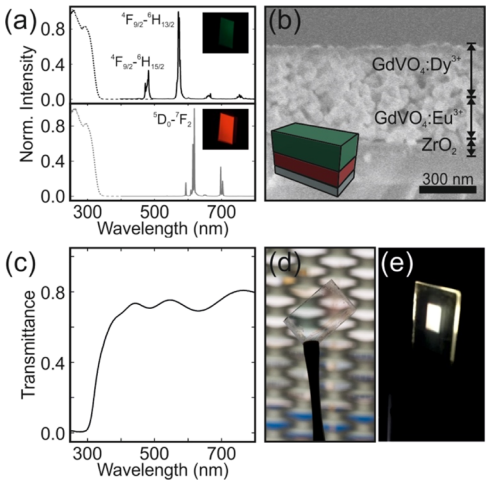

Figure 2. Normalized PL spectra of $GdVO_4$:Dy^{3+} (solid black line) and $GdVO_4$:Eu^{3+} films (solid gray line) when illuminated at 295 nm; photoexcitation spectra attained while detecting at 572 nm (dashed black line) or 615 nm (dashed gray line). Pictures of the emission color of films illuminated at 295 nm are shown as insets. (b) FESEM image of a cross section of the layered phosphor coating made by the sequential deposition of $GdVO_4$:Dy^3 and $GdVO_4$:Eu^3 nanophosphor layers followed by sintering. (c) Ballistic transmittance spectrum of the layered phosphor coating. (d,e) Photographs of the same film under natural and UV light.

by sequential spin coating of nanophosphors. To improve the adhesion to the substrate (quartz), the phosphor bilayer is deposited over a thin layer of ZrO_2. We observed that such a layer improves the uniformity of the nanophosphor films deposited atop, which may originate from the different surface charge of the ZrO_2 film compared to the quartz substrate. To achieve white-light emission, stacks with a total thickness of ∼500 nm were prepared, so that full extinction of the photoexcitation was guaranteed as it would be required if these coatings are integrated as downshifters in light-emitting devices. Indeed, our measurements indicate that the PL intensity increases with the thickness of the films up to ∼350 nm, meaning that such value of film thickness is enough so as to absorb the complete fraction of the excitation light that is not reflected in the nanophosphor/air interface.[17] Eventually, layered coatings were sintered at 800 °C. Thermal annealing gives rise to porous but continuous films in which structural defects and surface traps present in the as-prepared nanocrystals are reduced.[17] A field emission scanning electron microscopy (FESEM) image of the cross section of one of these stacks is shown in Figure 2b. As the crystalline matrix hosting the two types of cations employed is the same, each layer in the stack responds equally to the thermal treatment, making the interface between the two types of RE-doped layers indistinguishable.

We determine the absolute values of the ballistic transmittance. The illustrative results attained for a bilayer stack composed of ∼300 nm of $GdVO_4$:Dy^{3+} and ∼200 nm of $GdVO_4$:Eu^{3+} are shown in Figure 2c. The transmittance remains above 70% for the complete visible range, with oscillations that arise as a result of the optical interference occurring in the layered stack. The fraction of light absorbed by the bilayer reaches 70% in the UV range at which the phosphors of choice are excited, with the remaining light at these short wavelengths diffusely scattered by the disordered pore network present in the sintered films. Hence, although the

DOI: 10.1021/acsami.8b17368
ACS Appl. Mater. Interfaces 2019, 11, 4219−4225

random porous network observable in the bulk of the film does not give rise to diffuse visible light, it scatters shorter wavelength photons to some non-negligible extent. The transparency (τ) of the stacks can be formally estimated with the expression (ISO 9050:2003)

$$\tau = \frac{\int_{\lambda_1}^{\lambda_2} T(\lambda)F(\lambda)P(\lambda)\,\mathrm{d}\lambda}{\int_{\lambda_1}^{\lambda_2} F(\lambda)P(\lambda)\,\mathrm{d}\lambda} \quad (1)$$

where $P(\lambda)$ is the photopic spectral luminous efficiency function, which represents the sensitivity of an observer in photometry (ISO/CIE 10527), and F is the AM1.5 solar spectral irradiance. The values of τ for all coatings were basically the same and around 75%. The pictures displayed in Figure 2d,e confirm that the resulting films are highly transparent and emit white light when illuminated with an adequate UV light. Notice that UV LEDs in combination with phosphor mixtures typically provide sources with a higher color-rendering index, which could potentially minimize light pollution.

The photophysical properties of the coatings were studied by means of photoexcitation and PL spectroscopies using a spectrofluorometer (Edinburgh FLS1000). The excitation wavelength (λ_{ex}) was varied from 250 to 320 nm. The results for a particular configuration, namely a bilayer stack composed of ~300 nm of $GdVO_4$:Dy^{3+} and ~200 nm of $GdVO_4$:Eu^{3+} annealed films, are shown in Figure 3a. Notice that the thickness of each nanophosphor layer can be precisely controlled through the concentration of the nanophosphor dispersion and the deposition speed. As a result, the film thickness can be processed with a precision of a few nanometers. Interestingly, the PL spectra are extremely dependent on the excitation wavelength. This is a direct consequence of the layered structure of the coating. In the selected example, light encounters first the $GdVO_4$:Dy^{3+} layer and then the $GdVO_4$:Eu^{3+} one. The shorter the wavelength, the smaller is the penetration depth in the stack. Hence, for 250 nm $\leq \lambda_{ex} \leq$ 290, all incoming intensities are practically absorbed by the $GdVO_4$:Dy^{3+} layer and hardly reach the second $GdVO_4$:Eu^{3+} layer. Hence, the features of Dy^{3+} dominate over those of Eu^{3+} in the PL spectrum. As the photoexcitation wavelength increases, the penetration depth also increases, and the balance between the contributions from both species improves, as it can be seen for those spectra attained when photoexciting with 295 nm $\leq \lambda_{ex} \leq$ 320. This is further illustrated in Figure 3b, in which the PL spectra attained when illuminating the same bilayer at either λ = 275 nm (black) or λ = 300 nm (gray) are plotted. Although both emissions lie in the achromatic region of the chromaticity space, their spectral composition is very different. Remarkably, the tuning of the emission shade is not achieved at the expense of a significant reduction of the amount of emitted light. Indeed, although the extinction coefficient of the phosphor reduces by 60% from λ_{ex} = 265 nm to λ_{ex} = 320 nm, the total emitted light only diminishes by 15% when photoexciting at λ_{ex} = 320 nm. Figure 3c shows the time-dependent PL of the $^4F_{9/2}$ level of Dy^{3+} and the $^5D_0$ level of Eu^{3+} activators when they form an isolated film and when such films are stacked in a bilayer. Our results indicate that the structuring of the phosphors does not alter their dynamics, and the associated lifetimes are nearly identical. Indeed, the fitting of the decay curves yields the average lifetimes of 0.22 and 0.94 ms for Dy^{3+} and Eu^{3+}, respectively. The QY of the Dy^{3+} layer is ~25%, whereas the Eu^{3+} film features an efficiency of ~75%, which gives rise to QYs above 35% for the stack, as shown in Figure 3d.

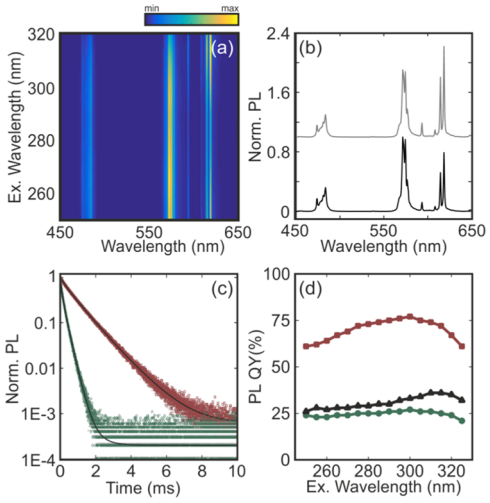

Figure 3. (a) PL spectra attained from a layered phosphor stack when the photoexcitation wavelength is gradually varied between 250 and 320 nm. All curves are normalized to the maximum intensity attained at 572 nm when the stack is illuminated at 265 nm. (b) PL spectrum of the stack illuminated at 275 nm (black) and 300 nm (gray). The gray curve has been vertically shifted for the sake of clarity. (c) Time-dependent PL of the $^4F_{9/2}$ and $^5D_0$ levels of Dy^{3+} (green symbols) and Eu^{3+} activators (red symbols) in the stack, respectively, together with their corresponding fits to the sum of two log-normal distributions of decay rates (black solid lines). Time dependence of the same transitions when the activators are deposited as isolated films is also shown as dark and light gray symbols, respectively. (d) PL QY vs the photoexcitation wavelength for a $GdVO_4$:Dy^{3+} layer (green symbols), a $GdVO_4$:Eu^{3+} layer (red symbols), and a $GdVO_4$:Dy^{3+}/$GdVO_4$:Eu^{3+} stack (black symbols).

The particular photochromic effect displayed herein offers a unique and unprecedented way to control the shade of the emission color attained from a phosphor coating. In this regard, the potential of these transparent stacks is analyzed by studying the PL of the $GdVO_4$:Dy^{3+}/$GdVO_4$:Eu^{3+} stack in comparison with a 500 nm film in which $GdVO_4$:Dy^{3+} and $GdVO_4$:Eu^{3+} phosphor nanoparticles were mixed together at two different ratios. A gradual shift of the excitation energy allows attaining different chromaticity values comprised between the one of $GdVO_4$:Dy^{3+} and $GdVO_4$:Eu^{3+}—open symbols in Figure 4a. As it can be seen in the CIE 1931 color space plotted in Figure 4a, a variety of shades contained in the achromatic region are achieved. In particular, the photoexcitation of the $GdVO_4$:Dy^{3+}/$GdVO_4$:Eu^{3+} stack at λ_{ex} = 300 nm yields a warm white light, meeting the Planckian locus at 2600 K. Similarly, when the order of the layers in the stack is reversed, that is, $GdVO_4$:Eu^{3+}/$GdVO_4$:Dy^{3+}, the color of the emission can be also controlled with the photoexcitation wavelength, as shown with red symbols in Figure 4a. In contrast, when the $GdVO_4$:Dy^{3+} and $GdVO_4$:Eu^{3+} phosphor nanoparticles are mixed together in a film, the chromaticity of the emission is only determined by the ratio of each material in the mix, for example, 85% of $GdVO_4$:Dy^{3+} or 60% of $GdVO_4$:Dy^{3+} nanophosphors, and the color coordinates of the homogeneous mixture are independent of the photoexcitation wavelength, as shown by dark and gray symbols in

DOI: 10.1021/acsami.8b17368
ACS Appl. Mater. Interfaces 2019, 11, 4219−4225

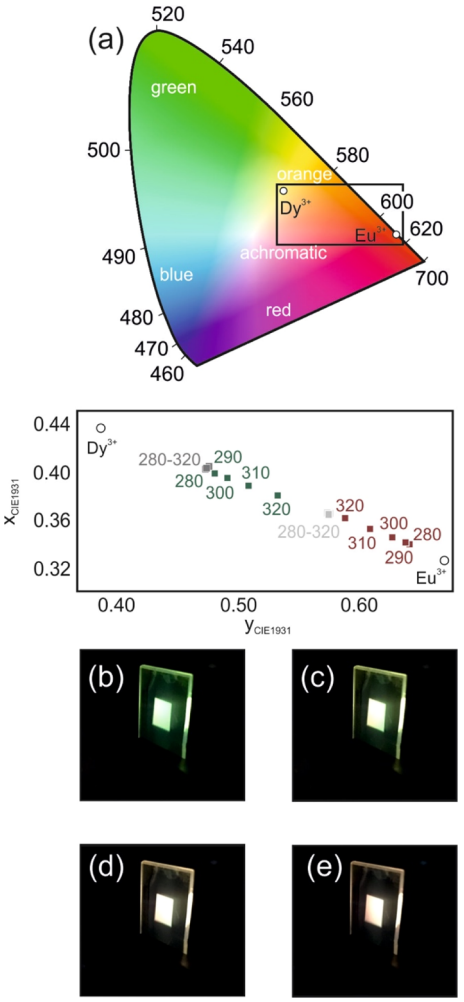

Figure 4. (a) CIE 1931 chromaticity coordinates of the light emitted by a $GdVO_4$:Dy^{3+}/$GdVO_4$:Eu^{3+} stack (green symbols) and a $GdVO_4$:Eu^{3+}/$GdVO_4$:Dy^{3+} stack bilayer (red symbols) as a function of the photoexcitation wavelength. Color coordinates of a mixture $GdVO_4$:Dy^{3+}/$GdVO_4$:Eu^{3+} with 85% (dark gray symbols) and 60% of Dy^{3+} (light gray symbols) along with the coordinates of the $GdVO_4$:Dy^{3+} and $GdVO_4$:Eu^{3+} layers (open circles) are also shown. (b–e) Digital pictures of the PL of a $GdVO_4$:Dy^{3+}/$GdVO_4$:Eu^{3+} phosphor bilayer for four different photoexcitation wavelengths: 280 (b), 290 (c), 300 (d), and 310 nm (e).

Figure 4a, which highlights the importance of the phosphor layering to tune the emission color of a given film. Notice that we did not consider preparing films of codoped $GdVO_4$:Dy^{3+}/Eu^{3+} nanophosphors to avoid processes related to cross-relaxation and energy transfer between the energy levels of Dy^{3+} and Eu^{3+}, which generally deteriorate the yield of the individual activators. Finally, Figure 4b–e displays the digital pictures of the light emitted by the coatings, which highlight the precision in determining the coating response that can be achieved by combining the adequate bilayer configuration and excitation wavelength. We have demonstrated that both routes (mixing and layering) allow tuning the emission color of a combination of phosphors. Indeed, our measurements confirm that chromaticity coordinates can be accurately controlled by engineering the relative ratio between the Dy^{3+} and Eu^{3+} nanoparticles in the mixture. However, different emission colors require the preparation of different coatings. In contrast, the layering approach offers the possibility to tune the chromaticity of the emission of a given coating by changing the photoexcitation wavelength, which represents its main benefit.

In conclusion, $GdVO_4$ was proved to be the best host for Eu^{3+} ions over the $NaGd(WO_4)_2$, $NaGd(MoO_4)_2$, and $LaVO_4$ materials. We have also demonstrated a synthetic route to attain a transparent white-light-emitting coating based on a layered phosphor structure.

The choice of materials determines the range of white shades in which the chromaticity can be tuned. In our demonstration, we choose two nanophosphors that yield warm white light (2600 K) when combined in a stack that is photoexcited with light of 300 nm. High efficiency as well as a dynamic chromatic tuning of PL has been shown. The combination of these features with the level of transparency achieved allows us to foresee a great potential impact of the approach proposed herein in the field of solid-state lighting and displays. These novel color-converting coatings are also easily processed and are versatile in terms of the substrate they can be deposited on. Future developments must target the development of layered phosphor coatings that can be efficiently photoexcited at longer wavelengths, for which more efficient electroluminescence sources exist, so that a high electrical-to-luminous power conversion ratio can be achieved.

3. EXPERIMENTAL SECTION

3.1. Materials. Gadolinium(III) nitrate hexahydrate [$Gd(NO_3)_3 \cdot 6H_2O$, Aldrich, 99.9%], lanthanum(III) nitrate hydrate [$La(NO_3)_3 \cdot xH_2O$, Aldrich, 99.9%], europium(III) nitrate pentahydrate [$Eu(NO_3)_3 \cdot 5H_2O$, Aldrich, 99%], dysprosium(III) nitrate hydrate [$Dy(NO_3)_3 \cdot xH_2O$, Aldrich, 99.9%], sodium orthovanadate (Na_3VO_4, Aldrich, 99.9%), sodium tungstate dihydrate ($Na_2WO_4 \cdot 2H_2O$, Aldrich, ≥99%), sodium molybdate (Na_2MoO_4, Aldrich, ≥98%), sodium citrate (Na_3Cit, $Na_3C_6O_7H_5 \cdot 2H_2O$, Aldrich, 99.5%), PAA (average $M_w \approx 1800$, Aldrich), ethylene glycol, zirconium(IV) *n*-propoxide 70% in 1-propanol (Aldrich), triblock copolymers Pluronic F127 ($M_w \approx 12\,600$), 2,4-pentanedione (acetylacetonate, Alfa Aesar), absolute ethanol, methanol, HCl (3.571 mol·L^{-1}, Panreac), and Milli-Q water.

3.2. Nanophosphor Synthesis. We synthesized $NaGd(WO_4)_2$:Eu^{3+}, $NaGd(MoO_4)_2$:Eu^{3+}, $LaVO_4$:Eu^{3+}, $GdVO_4$:Eu^{3+}, and $GdVO_4$:Dy^{3+} nanophosphors following a procedure described elsewhere.[23−26] The optimized doping concentrations of Eu^{3+} in each of these nanophosphors are, respectively, 12, 5, 5, and 10%. The doping concentration of Dy^{3+} in the $GdVO_4$ matrix was fixed at 2%.[17] The nanophosphors were dispersed in methanol with a concentration of 5% by wt.

3.3. Preparation of Nanophosphor Coatings. First, a ZrO_2 precursor sol was prepared following a synthesis reported elsewhere.[17] Then, a thin ZrO_2 film was deposited over a quartz substrate by spin coating (Laurell WS-400) using 190 μL of the ZrO_2 precursor sol with an acceleration ramp of 11 340 rpm s^{-1} and a final rotation speed of 3000 rpm. The film was annealed at 400 °C for 10 min. Subsequently, the nanophosphor layers were deposited by spin coating using 180 μL of nanophosphor dispersion with an acceleration ramp of 11 340 rpm s^{-1} and a final rotation speed between 1500 and 3000 rpm. To obtain layers of different thicknesses, several nanophosphor layers were deposited using the same deposition conditions. Finally, the as-prepared nanophosphor coatings were annealed at 800 °C for 4 h.

3.4. Characterization. Scanning electron microscopy (SEM) images of the top view and cross section of the nanophosphor films deposited onto quartz were taken by using a Hitachi S4800 microscope. The crystalline structure of the as-prepared nanophosphors was investigated by XRD (PANalytical X'pert Pro). The excitation and emission spectra as well as the lifetime of these samples

DOI: 10.1021/acsami.8b17368
ACS Appl. Mater. Interfaces 2019, 11, 4219−4225

were measured with Edinburgh Instruments (FLS1000). The ballistic transmittance of nanophosphor films was recorded using a Cary 7000 series UV−vis−NIR spectrophotometer. The QY values were measured from the ratio between the light emitted and light absorbed by the nanophosphor films. Thus, they comprise processes from the absorption of the excitation light by the nanophosphor matrix to the transfer to the RE activator and the subsequent outcoupling to free space of the emitted light. The measurements were performed using an integrating sphere attached to FLS 1000.

AUTHOR INFORMATION

Corresponding Authors

*E-mail: g.lozano@csic.es (G.L.).
*E-mail: h.miguez@csic.es (H.M.).

ORCID

Gabriel Lozano: 0000-0002-0235-4924
Hernán Míguez: 0000-0003-2925-6360

Author Contributions

The manuscript was written with contributions from all authors. All authors have given approval to the final version of the manuscript.

Funding

Spanish Ministry of Economy and Competitiveness grant MAT2017-88584-R; European Research Council (ERC) under the European Union's Horizon 2020 research and innovation program, grant agreement no. 715832.

Notes

The authors declare no competing financial interest.

ACKNOWLEDGMENTS

This project has received funding from the European Research Council (ERC) under the European Union's Horizon 2020 research and innovation program (NANOPHOM, grant agreement no. 715832) and the Spanish Ministry of Economy and Competitiveness under grant MAT2017-88584-R.

REFERENCES

(1) Xia, Z.; Liu, Q. Progress in Discovery and Structural Design of Color Conversion Phosphors for LEDs. *Prog. Mater. Sci.* **2016**, *84*, 59−117.

(2) Ye, S.; Xiao, F.; Pan, Y. X.; Ma, Y. Y.; Zhang, Q. Y. Phosphors in Phosphor-Converted White Light-Emitting Diodes: Recent advances in materials, techniques and properties. *Mater. Sci. Eng., R* **2010**, *71*, 1−34.

(3) Murai, S.; Verschuuren, M. A.; Lozano, G.; Pirruccio, G.; Koenderink, A. F.; Rivas, J. G. Enhanced Absorption and Emission of $Y_3Al_5O_{12}$:Ce^{3+} Thin Layers Prepared by Epoxide-Catalyzed Sol-Gel Method. *Opt. Mater. Express* **2012**, *2*, 1111−1120.

(4) Murai, S.; Sato, T.; Yao, S.; Kamakura, R.; Fujita, K.; Tanaka, K. Fabrication of Cerium-Doped Yttrium Aluminum Garnet Thin Films by a Mist CVD Method. *J. Lumin.* **2016**, *170*, 808−811.

(5) Santana-Alonso, A.; Méndez-Ramos, J.; Yanes, A. C.; del-Castillo, J.; Rodríguez, V. D. White Light Up-Conversion in Transparent Sol−Gel Derived Glass-Ceramics Containing Yb^{3+}−Er^{3+}−Tm^{3+} Triply-Doped YF_3 Nanocrystals. *Mater. Chem. Phys.* **2010**, *124*, 699−703.

(6) Chen, D.; Xiang, W.; Liang, X.; Zhong, J.; Yu, H.; Ding, M.; Lu, H.; Ji, Z. Advances in transparent glass-ceramic phosphors for white light-emitting diodes-A review. *J. Eur. Ceram. Soc.* **2015**, *35*, 859−869.

(7) Liu, L.; Yu, M.; Zhang, J.; Wang, B.; Liu, W.; Tang, Y. Facile Fabrication of Color-Tunable and White Light Emitting Nano-Composite Films Based on Layered Rare-Earth Hydroxides. *J. Mater. Chem. C* **2015**, *3*, 2326−2333.

(8) Zhou, S.; Jiang, N.; Zhu, B.; Yang, H.; Ye, S.; Lakshminarayana, G.; Hao, J.; Qiu, J. Multifunctional Bismuth-Doped Nanoporous Silica Glass: From Blue-Green, Orange, Red, and White Light Sources to Ultra-Broadband Infrared Amplifiers. *Adv. Funct. Mater.* **2008**, *18*, 1407−1413.

(9) Shen, T.; Zhang, Y.; Liu, W.; Tang, Y. Novel Multi-Color Photoluminescence Emission Phosphors Developed by Layered Gadolinium Hydroxide via in situ Intercalation with Positively Charged Rare-Earth Complexes. *J. Mater. Chem. C* **2015**, *3*, 1807−1816.

(10) Lee, K.-H.; Lee, B.-I.; You, J.-H.; Byeon, S.-H. Transparent Gd_2O_3:Eu Phosphor Layer Derived from Exfoliated Layered Gadolinium Hydroxide Nanosheets. *Chem. Commun.* **2010**, *46*, 1461−1463.

(11) Meyer, L. V.; Schönfeld, F.; Müller-Buschbaum, K. Lanthanide based tuning of luminescence in MOFs and dense frameworks - from mono- and multimetal systems to sensors and films. *Chem. Commun.* **2014**, *50*, 8093−8108.

(12) Liu, Y.; Liu, G.; Dong, X.; Wang, J.; Yu, W. Tunable Photoluminescence and Magnetic Properties of Dy^{3+} and Eu^{3+} Doped $GdVO_4$ Multifunctional Phosphors. *Phys. Chem. Chem. Phys.* **2015**, *17*, 26638−26644.

(13) Giaume, D.; Poggi, M.; Casanova, D.; Mialon, G.; Lahlil, K.; Alexandrou, A.; Gacoin, T.; Boilot, J.-P. Organic Functionalization of Luminescent Oxide Nanoparticles toward Their Application As Biological Probes. *Langmuir* **2008**, *24*, 11018−11026.

(14) Gupta, B. K.; Rathee, V.; Narayanan, T. N.; Thanikaivelan, P.; Saha, A.; Govind; Singh, S. P.; Shanker, V.; Marti, A. A.; Ajayan, P. M. Probing a Bifunctional Luminomagnetic Nanophosphor for Biological Applications: a Photoluminescence and Time-Resolved Spectroscopic Study. *Small* **2011**, *7*, 1767−1773.

(15) Laguna, M.; Nuñez, N. O.; Becerro, A. I.; Ocaña, M. Morphology Control of Uniform $CaMoO_4$ Microarchitectures and Development of White Light Emitting Phosphors by Ln Doping (Ln = Dy^{3+}, Eu^{3+}). *CrystEngComm* **2017**, *19*, 1590−1600.

(16) Wang, Y.; Tang, J.; Huang, X.; Jiang, L. Luminescence Properties of Eu^{3+}:$NaGd(WO_4)_2$ Nanoparticles and Nanorods. *J. Rare Earths* **2016**, *34*, 118−124.

(17) Park, J.-S.; Kim, J. K.; Cho, J.; Seong, T.-Y. Review-Group III-Nitride-Based Ultraviolet Light-Emitting Diodes: Ways of Increasing External Quantum Efficiency. *ECS J. Solid State Sci. Technol.* **2017**, *6*, Q42−Q52.

(18) Geng, D.; Lozano, G.; Calvo, M. E.; Núñez, N. O.; Becerro, A. I.; Ocaña, M.; Míguez, H. Photonic Tuning of the Emission Color of Nanophosphor Films Processed at High Temperature. *Adv. Opt. Mater.* **2017**, *5*, 1700099.

(19) Geng, D.; Cabello-Olmo, E.; Lozano, G.; Míguez, H. Photonic Structuring Improves the Colour Purity of Rare-Earth Nano-phosphors. *Mater. Horiz.* **2018**, *5*, 661−667.

(20) Brik, M. G. Influence of Chemical Bond Length Changes on the Crystal Field Strength and "Ligand−Metal" Charge Transfer Transitions in Cs_2GeF_6 Doped with Mn^{4+} and Os^{4+} Ions. *J. Phys. Chem. Solids* **2007**, *68*, 1341−1347.

(21) Kodaira, C. A.; Brito, H. F.; Malta, O. L.; Serra, O. A. Luminescence and Energy Transfer of the Europium (III) Tungstate Obtained via the Pechini method. *J. Lumin.* **2003**, *101*, 11−21.

(22) Binnemans, K. Interpretation of Europium(III) Spectra. *Coord. Chem. Rev.* **2015**, *295*, 1−45.

(23) Laguna, M.; Escudero, A.; Núñez, N. O.; Becerro, A. I.; Ocaña, M. Europium-Doped $NaGd(WO_4)_2$ Nanophosphors: Synthesis, Luminescence and Their Coating with Fluorescein for pH Sensing. *Dalton Trans.* **2017**, *46*, 11575−11583.

(24) Laguna, M.; Nuñez, N. O.; Rodríguez, V.; Cantelar, E.; Stepien, G.; García, M. L.; de la Fuente, J. M.; Ocaña, M. Multifunctional Eu-doped $NaGd(MoO_4)_2$ Nanoparticles Functionalized with Poly(L-lysine) for Optical and MRI Imaging. *Dalton Trans.* **2016**, *45*, 16354−16365.

(25) Nuñez, N. O.; Zambrano, P.; García-Sevillano, J.; Cantelar, E.; Rivera-Fernández, S.; de la Fuente, J. M.; Ocaña, M. Uniform Poly(acrylic acid)-Functionalized Lanthanide-Doped $LaVO_4$ Nano-

DOI: 10.1021/acsami.8b17368
ACS Appl. Mater. Interfaces 2019, 11, 4219−4225

phosphors with High Colloidal Stability and Biocompatibility. *Eur. J. Inorg. Chem.* **2015**, 4546−4554.
(26) Nuñez, N. O.; Rivera, S.; Alcantara, D.; de la Fuente, J. M.; García-Sevillano, J.; Ocaña, M. Surface Modified Eu:$GdVO_4$ Nanocrystals for Optical and MRI Imaging. *Dalton Trans.* **2013**, *42*, 10725−10734.

DOI: 10.1021/acsami.8b17368
ACS Appl. Mater. Interfaces 2019, 11, 4219−4225